Permeability calculation of a fibrous thermal insulator using the Lattice Boltzmann method

Michel Ho[1], Sébastien Leclaire[1], Jean-Yves Trépanier[1], Marcelo Reggio[1], and Alexandre Martin[2]

[1]*Polytechnique Montréal, Montréal, Québec, H3T 1J4, Canada*
[2]*University of Kentucky, Lexington, Kentucky, 40506*

Abstract

The Lattice Boltzmann method is used to compute the permeability of FiberForm, a fibrous thermal insulator commonly used as the substrate of thermal protection systems materials. The results are compared to experiment and numerical results that uses another approach. The Lattice Boltzmann approach proves to be as accurate as the other computational methods, but shows a computational efficiency that is orders of magnitude smaller.

1 Introduction

The high speed at which a spacecraft travels during atmospheric reentry generates a large amount of heat that can cause serious damage. Porous heat shields mitigate the incidental energy flux through various ablation processes and their microstructure improves heat dissipation through several process, one of which is convective cooling [1]. Among various thermal protection systems (TPS), phenolic impregnated carbon ablator (PICA) has proven effective and efficient on several missions [2–4]. An important parameter required to assess the thermal protection ability of this class of TPS is permeability, which characterizes fluid transport within the micro-pores [5–8]. Here, the lattice Boltzmann method is applied to calculate the transverse isotropic permeability of a micro-computed tomography (µCT) reconstruction of FiberForm, PICA's porous fibrous substrate.

2 Numerical method and geometry

The lattice Boltzmann method (LBM) is a meso-scale CFD approach based on a discretized form of the Boltzmann transport equation that can recover hydrodynamic equations through the Chapman-Enskog expansion [9, 10]. Its algorithm allows an easy treatment of complex solid boundaries on a regular Cartesian grid [11, 12], and local calculation of macroscopic quantities enables efficient parallel computing [13, 14]. These features makes the LBM particularly suitable for fluid flow simulation through fibrous porous materials with highly-complex microstructure.

The LBM performs fluid simulations using non-dimensional variables. However, the real fluid behavior (and thus variables in physical units) can be recovered if the dimensionless quantities of interest are respected. This study features single phase gas flow through a fibrous structure in the hydrodynamic regime. Within these assumptions, only the Reynolds number may affect the flow regime and thus the intrinsic permeability value [15, 16]. Since Darcy's law is used to extract the permeability values, inertial effects of the flow are neglected, and the numerical Reynolds number must thus be low enough to ensure a creeping flow.

The geometry investigated in this work is a µCT reconstruction of FiberForm — the carbon fiber substrate of PICA. Details of the digitization are explained in Ref. [17]. The µCT image was obtained in gray-scale values from 0 to 255 and a threshold value of 106.5 was imposed to differentiate fluid voxels from solid. This value sets the voxelized geometry, shown in Fig. 1, to a porosity of $\simeq 0.87$, consistent with FiberForm [18]. The structure is cubic, with an edge length $\hat{L} = 520$ µm, and a mean fiber diameter of 11 µm. Because of the manufacturing process [19], the sample displays a degree of symmetry, with fibers uniformly oriented in the plane orthogonal to the compression axis (identified as the Through-Thickness (TT) direction) and randomly oriented in the plane (identified as the In-Plane (IP) direction) [18]. The transverse isotropic nature of the geometry is expected to result in transverse isotropic fluid transport properties.

The results presented here were computed using an in-house code that uses the *ArrayFire* library [20] to enable faster GPU computations. The computational domain is composed of the voxelized geometry surrounded by two buffer fluid zones of width $\hat{W} = 52$ µm in the direction parallel to the flow. Pressure regularized boundary conditions [21] are applied at the inlet and the outlet of the domain, whereas periodic boundary conditions are imposed on the lateral faces of the domain. The inlet to outlet pressure ratio is kept sufficiently low to respect the constraint on the Reynolds number given previously, and remains constant throughout the different structure orientations. Solid walls are treated with the standard *fullway bounce-back* boundary condition [9]. A D3Q19 scheme is used for the velocity discretization and a simple relaxation time (SRT) collision operator is used in the LBM algorithm [9], and is set to unity. This specific value is chosen as, when combined with the bounce-back boundary condition, it correctly accounts for the position of the wall [22, 23].

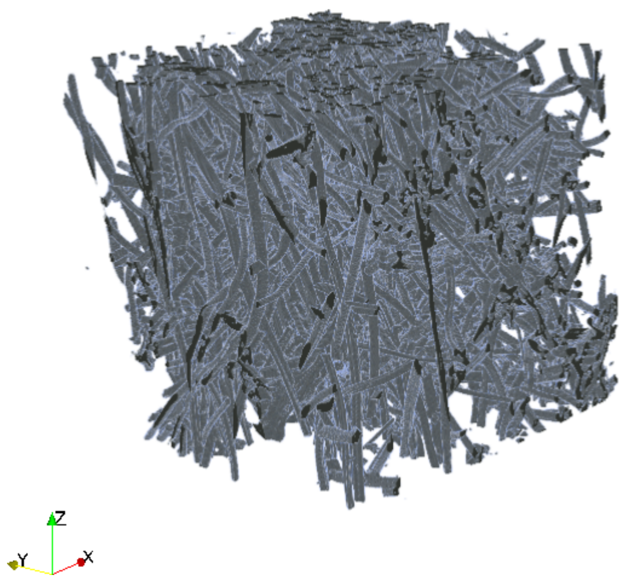

Figure 1: Voxelized representation of a FiberForm sample, obtained by x-ray micro-computed tomography [24]. TT orientation is along x-axis, IP orientations are in the yz-plane.

3 Simulations results

To establish the permeability matrix of the sample, fluid simulations were performed on both TT and IP orientations by re-orienting the porous sample without changing the direction of the pressure gradient. In a similar fashion to the results presented in Ref. [17], the sample was discretized to 400×400×400 voxels with an additional 40 voxels for each buffer zone, resulting in a voxel resolution of 1.3 µm.

Fig. 2 shows the normalized velocity contours for TT and IP FiberForm orientations at mid-planes. The velocity was normalized by the maximum velocity in the fluid domain for the TT orientation. It can be seen that the IP configuration is more permeable than the TT configuration, as the contours exhibit a higher flow velocity despite the same pressure gradient. More specifically, the IP orientation exhibits a large region at high velocity, parallel to the flow direction. Because of the disposition of the fibers, the IP orientation exhibits less resistance to the flow, and translates into a high velocity inflow.

The flow behavior with respect to the orientation of the sample is also featured in Fig. 3, where permeability values are displayed for the two orientations. The results were compared to Direct Simulation Monte-Carlo (DSMC) results obtained by Borner et al. [17] and Jambunathan et al. [25], using the same micro-CT scan. Experimental data provided by Panerai et al. [18], obtained on several FiberForm samples, are also displayed for comparison. For the TT orientation, the LBM computations show

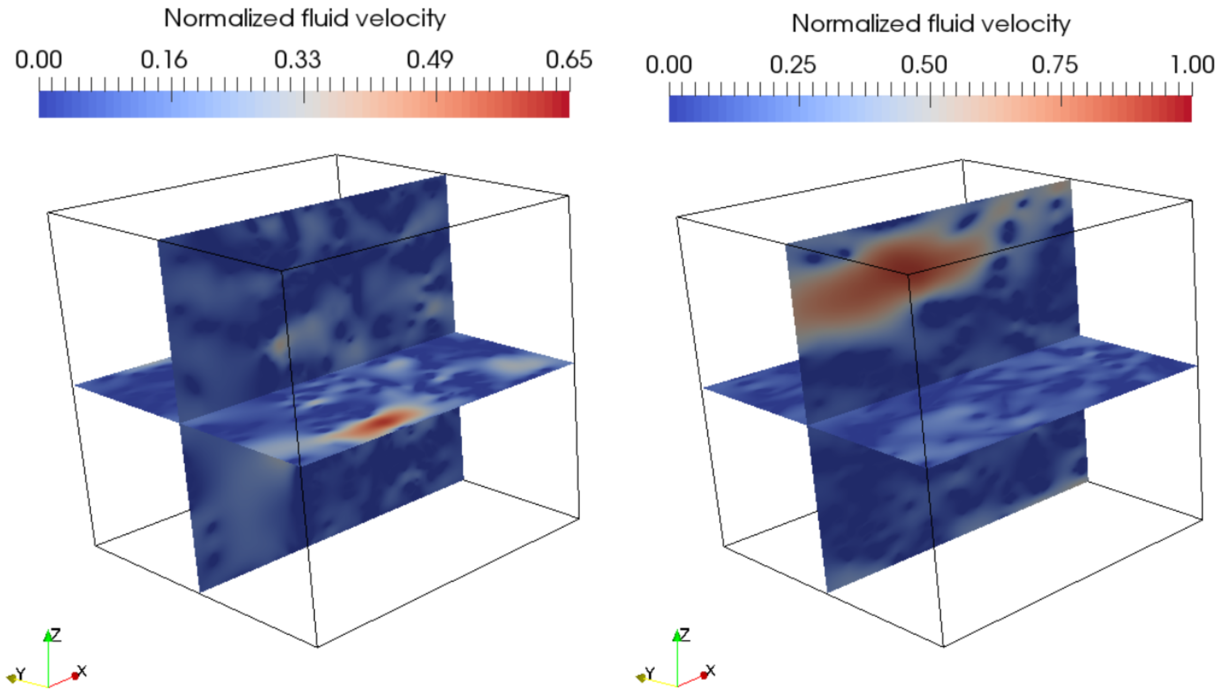

Figure 2: Normalized velocity contours for TT (left) and IP (right) oriented FiberForm for pressure driven Argon flow. Featured planes are parallel to the flow direction. Dark blue spots depict zero fluid velocity.

close permeability values with both DSMC results, which is is expected as all numerical simulations were performed on the same geometry. All computed values lie well within the range of the measured permeability values. In regards to the IP orientation, the LBM results are similar to those of Borner et al. [17], but show an appreciable disparity from those of Jambunathan et al. [25]. The validity of the computed results are difficult to assess since only one experimental measurement is available in Ref. [18]. The permeability of FiberForm was also measured in Ref. [26], and modeled with DSMC in Ref. [27], using samples with different densities (and thus porosities) than the one used here.

The complete permeability matrix $\hat{\boldsymbol{K_0}}$ can be recovered by performing fluid flow simulations along the second IP orientation and applying Darcy's law:

$$\hat{\boldsymbol{K_0}} = \begin{bmatrix} 50.78 & 0.018 & 0.013 \\ 0.018 & 68.16 & 0.003 \\ 0.013 & 0.003 & 96.50 \end{bmatrix} \tag{1}$$

The off-diagonal terms are several orders of magnitude smaller than the diagonal terms, suggesting that the sample was well aligned to the manufactured plane when imaged. To that point, a re-orientation of the sample along the principal axis results in permeability values of $K_{\mathrm{TT}} = 50.78$, $K_{\mathrm{IP},1} = 68.16$, $K_{\mathrm{IP},2} = 96.50$, which are identical (to the same degree of precision) to the diagonal terms of the matrix. However, the sample does not appears to be as transverse-isotropic as anticipated. Even though the TT orientation exhibits a lower permeability than that of the two IP orientation, the y-axis permeability is significantly lower than that along the z-axis. This, however, is expected since FiberForm is known to have large geometric variability across multiple length scales [18]. True transverse isotropy should not be expected unless a wide distribution of sample geometries are studied, as highlighted in [28–30].

A drawback of the LB algorithm when computing permeability is the approximation of solid surfaces with voxels. To assess the influence of voxel resolution on permeability calculation, a grid refinement study was performed. Similar to Borner et al. [17], permeability calculations were performed using the same geometry but with varied grayscale threshold values, and, subsequently, different porosities. Table 1 shows computational data for a range of voxel resolutions. It is observed that the relative error in permeability values is still significant, even for a discretization of 200 nodes per length, and that this relative error is higher for the TT orientation.

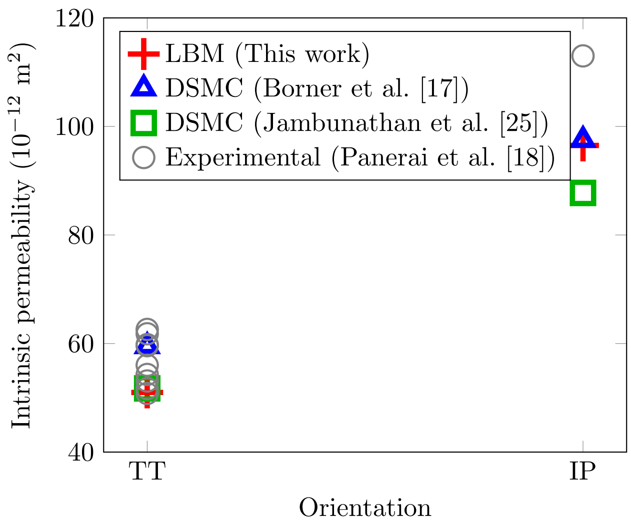

Figure 3: Intrinsic permeability values for TT and IP FiberForm orientations.

However, these results must be thoughtfully considered given the way the voxelized geometry is coarsened. In order to keep the porosity value constant, the threshold value must be changed from one grid size to another. Therefore, dissimilar voxelations methods may result in dissimilar microstructures and pore connectivities, significantly affecting the final permeability. A Richardson extrapolation performed using the more refined results indicates that the 1.3 µm resolution (*i.e.* 400 nodes per length) are converged within a few percent. The resolution of 2.6 µm (*i.e.* 200 nodes per length), which gives an accuracy below 15%, could still be considered adequate for first order computations, since the computed time is significantly lower. Overall, the results show the ability of the LBM to compute permeability with great accuracy despite the approximation of fiber surfaces. Although the results presented here are in the continuum regime, the method can also be used in the rarefied regime [31].

Finally, a computation wall-time study was performed for the TT porosity of $\phi = 0.87$, with the results shown in Table 1. As seen, the 200×200×200 discretization is an excellent compromise between accuracy and computational efficiency. Since the simulation was able to be performed on a single GPU (AMD FirePro S9100 Hawaii 12GB 2015), the wall-time did not exceed one hour and the error was kept below 11%. The 400×400×400 simulations required the use of 8 GPUs which increased the computational cost, but increased the accuracy. Nevertheless, that wall-time remains orders of magnitude smaller than those obtained when using DSMC. Studies performed on similar materials reported wall-times of a few days, using ~ 100 cores [27, 32].

4 Conclusion

Pressure-driven fluid simulations were performed to compute the permeability of a micro-computed tomography reconstruction of FiberForm using the lattice Boltzmann method. Results were compared to experimental measurements and DSMC simulations and consistently showed good agreement. A grid refinement study on LBM simulations was conducted, showing that the numerical results were sensitive to the way the micro-computed tomography image was voxelized. The LBM results, using a voxel resolution of 1.3 µm, showed excellent agreement with the reference data. Moreover, the associated computational cost makes the method attractive as reasonable agreement can be obtained with the use of a single GPU, in less than one hour. The results presented here show that the LBM is an efficient and appropriate method for computing fluid transport properties through fibrous micro-porous thermal insulators.

Acknowledgments

Financial support for the first author was provided by the Simulation-based Engineering Science (Génie Par la Simulation) program funded through the CREATE program of the Natural Sciences and Engineering Research Council of Canada. This work was also supported by Mitacs through the Mitacs Globalink

Table 1: Intrinsic permeability values for different voxel resolutions and porosities. Relative permeability error is obtained by using a Richardson extrapolation as the reference value.

Porosity (m^3/m^3)	Nodes per length	Voxel size (μm)	Orientation	K (10^{-12} m^2)	Relative error (%)	Wall-time (hours)
0.847	100	5.2	TT	58.23	39	–
0.847	200	2.6	TT	48.01	15	–
0.847	400	1.3	TT	43.41	3.7	–
0.847	100	5.2	IP	104.5	28	–
0.847	200	2.6	IP	91.5	12	–
0.847	400	1.3	IP	84.1	3.0	–
0.87	100	5.2	TT	67.43	36	0.03
0.87	200	2.6	TT	54.73	10	0.29
0.87	400	1.3	TT	50.78	2.5	1.35
0.87	100	5.2	IP	116.3	22	–
0.87	200	2.6	IP	100.6	5.7	–
0.87	400	1.3	IP	96.5	1.4	–
0.9	100	5.2	TT	80.7	48	–
0.9	200	2.6	TT	62.25	14	–
0.9	400	1.3	TT	56.52	3.5	–
0.9	100	5.2	IP	131.9	30	–
0.9	200	2.6	IP	110.1	8.3	–
0.9	400	1.3	IP	103.8	2.1	–

Research Internship program (Award No: IT15256). The work presented here was also supported by Kentucky Space Grant – Research Initiation Award no. NNX15AR69H as well as NASA SpaceTech-REDDI-2017-ESI Award no. 80NSSC18K0261. Special thanks to M.J. Wright and M.D. Barnhardt (NASA Ames Research Center), as well as to T.S. Schwartzentruber (University of Minnesota) for facilitating this project. Finally, the authors are grateful to M.N. Seif for carefully reviewing the manuscript.

References

[1] Bowman, W. H., and Lawrence, R. M., "Ablative materials for high-temperature thermal protection of space vehicles," *Journal of Chemical Education*, Vol. 48, No. 10, 1971, pp. 690–691. doi:10.1021/ed048p690.

[2] Tran, H., Johnson, C., Rasky, D., Hui, F., Hsu, M.-T., and Chen, Y., "Phenolic impregnated carbon ablators (PICA) for Discovery Class missions," *31st Thermophysics Conference*, 1996, p. 1911. doi:10.2514/6.1996-1911.

[3] Edquist, K., Dyakonov, A., Wright, M., and Tang, C., "Aerothermodynamic design of the Mars Science Laboratory heatshield," *41st AIAA Thermophysics Conference*, 2009, p. 4075. doi:10.2514/6.2009-4075.

[4] Kontinos, D. A., and Wright, M. J., "Introduction: Atmospheric entry of the stardust sample return capsule," *Journal of Spacecraft and Rockets*, Vol. 47, No. 5, 2010, pp. 705–707. doi:10.2514/1.51522.

[5] Weng, H., Duzel, U., Fu, R., and Martin, A., "Geometric effects on charring ablator: modeling of the full-scale Stardust heat shield," *Journal of Spacecraft and Rockets*, 2020. doi:10.2514/1.A34828, in press.

[6] Weng, H., and Martin, A., "Numerical Investigation of Thermal Response Using Orthotropic Charring Ablative Material," *Journal of Thermophysics and Heat Transfer*, Vol. 29, No. 3, 2015, pp. 429–438. doi:10.2514/1.T4576.

[7] Weng, H., Bailey, S. C. C., and Martin, A., "Numerical study of iso-Q sample geometric effects on charring ablative materials," *International Journal of Heat and Mass Transfer*, Vol. 80, 2015, pp. 570–596. doi:10.2514/1.T4434.

[8] Weng, H., and Martin, A., "Multidimensional modeling of pyrolysis gas transport inside charring ablative materials," *Journal of Thermophysics and Heat Transfer*, Vol. 28, No. 4, 2014, pp. 583–597. doi:10.1016/j.ijheatmasstransfer.2014.09.040.

[9] Guo, Z., and Shu, C., *Lattice Boltzmann method and its applications in engineering*, Vol. 3, World Scientific, 2013. doi:10.1142/8806.

[10] Krüger, T., Kusumaatmaja, H., Kuzmin, A., Shardt, O., Silva, G., and Viggen, E. M., "The lattice Boltzmann method," *Springer International Publishing*, Vol. 10, 2017, pp. 978–3. doi:10.1007/978-3-319-44649-3.

[11] Wang, M., and Zhu, W., "Pore-scale study of heterogeneous chemical reaction for ablation of carbon fibers using the lattice Boltzmann method," *International Journal of Heat and Mass Transfer*, Vol. 126, 2018, pp. 1222–1239. doi:10.1016/j.ijheatmasstransfer.2018.05.133.

[12] Nabovati, A., Llewellin, E. W., and Sousa, A. C., "A general model for the permeability of fibrous porous media based on fluid flow simulations using the lattice Boltzmann method," *Composites Part A: Applied Science and Manufacturing*, Vol. 40, No. 6-7, 2009, pp. 860–869. doi:10.1016/j.compositesa.2009.04.009.

[13] Blair, S., Albing, C., Grund, A., and Jocksch, A., "Accelerating an MPI lattice Boltzmann code using OpenACC," *Proceedings of the second workshop on accelerator programming using directives*, 2015, pp. 1–9. doi:10.1145/2832105.2832111.

[14] Heuveline, V., Krause, M. J., and Latt, J., "Towards a hybrid parallelization of lattice Boltzmann methods," *Computers & Mathematics with Applications*, Vol. 58, No. 5, 2009, pp. 1071–1080. doi:10.1016/j.camwa.2009.04.001.

[15] Chai, Z., Shi, B., Lu, J., and Guo, Z., "Non-Darcy flow in disordered porous media: A lattice Boltzmann study," *Computers & Fluids*, Vol. 39, No. 10, 2010, pp. 2069–2077. doi:10.1016/j.compfluid.2010.07.012.

[16] Kundu, P., Kumar, V., and Mishra, I. M., "Experimental and numerical investigation of fluid flow hydrodynamics in porous media: Characterization of pre-Darcy, Darcy and non-Darcy flow regimes," *Powder Technology*, Vol. 303, 2016, pp. 278–291. doi:10.1016/j.powtec.2016.09.037.

[17] Borner, A., Panerai, F., and Mansour, N. N., "High temperature permeability of fibrous materials using direct simulation Monte Carlo," *International Journal of Heat and Mass Transfer*, Vol. 106, 2017, pp. 1318–1326. doi:10.1016/j.ijheatmasstransfer.2016.10.113.

[18] Panerai, F., White, J. D., Cochell, T. J., Schroeder, O. M., Mansour, N. N., Wright, M. J., and Martin, A., "Experimental measurements of the permeability of fibrous carbon at high-temperature," *International Journal of Heat and Mass Transfer*, Vol. 101, 2016, pp. 267–273. doi:10.1016/j.ijheatmasstransfer.2016.05.016.

[19] "Fiber Materials Inc." , 2014. URL `http://www.fibermaterialsinc.com/product/fiberform-rigidinsulation`.

[20] Yalamanchili, P., Arshad, U., Mohammed, Z., Garigipati, P., Entschev, P., Kloppenborg, B., Malcolm, J., and Melonakos, J., "ArrayFire - A high performance software library for parallel computing with an easy-to-use API," , 2015. URL `https://github.com/arrayfire/arrayfire`.

[21] Latt, J., Chopard, B., Malaspinas, O., Deville, M., and Michler, A., "Straight velocity boundaries in the lattice Boltzmann method," *Physical Review E*, Vol. 77, No. 5, 2008, p. 056703. doi:10.1103/PhysRevE.77.056703.

[22] Inamuro, T., Yoshino, M., and Ogino, F., "A non-slip boundary condition for lattice Boltzmann simulations," *Physics of fluids*, Vol. 7, No. 12, 1995, pp. 2928–2930. doi:10.1063/1.868766.

[23] Pan, C., Luo, L.-S., and Miller, C. T., "An evaluation of lattice Boltzmann schemes for porous medium flow simulation," *Computers & fluids*, Vol. 35, No. 8-9, 2006, pp. 898–909. doi:10.1016/j.compfluid.2005.03.008.

[24] Panerai, F., Ferguson, J. C., Lachaud, J. R., Martin, A., Gasch, M. J., and Mansour, N. N., "Micro-tomography based analysis of thermal conductivity, diffusivity and oxidation behavior of rigid and flexible fibrous insulators," *International Journal of Heat and Mass Transfer*, Vol. 108, Part A, 2017, pp. 801–811. doi:10.1016/j.ijheatmasstransfer.2016.12.048.

[25] Jambunathan, R., Levin, D. A., Borner, A., Ferguson, J. C., and Panerai, F., "Prediction of gas transport properties through fibrous carbon preform microstructures using Direct Simulation Monte Carlo," *International Journal of Heat and Mass Transfer*, Vol. 130, 2019, pp. 923–937. doi:10.1016/j.ijheatmasstransfer.2018.11.006.

[26] Marschall, J., and Milos, F. S., "Gas Permeability of Rigid Fibrous Refractory Insulations," *Journal of Thermophysics and Heat Transfer*, Vol. 12, No. 4, 1998, pp. 528–535. doi:10.2514/2.6372.

[27] Poovathingal, S., C.Stern, E., Nompelis, I., Schwartzentruber, T. E., and Candler, G. V., "Nonequilibrium flow through porous thermal protection materials, Part II: Oxidation and pyrolysis," *Journal of Computational Physics*, 2018. doi:10.1016/j.jcp.2018.02.043.

[28] McDaniel, S. M., Seif, M. N., Fu, R., Beck, M. J., and Martin, A., "Development of Stochastic Model for Fibrous Ablators," *59th AIAA Aerospace Sciences Meeting*, Nashville, TN, 2021. Submitted.

[29] Ho, M. F., Seif, M. N., McDaniel, S. M., Leclaire, S., Trépanier, J.-Y., Reggio, M., Beck, M. J., and Martin, A., "Fluid Behavior in Stochastic Porous Structures," *59th AIAA Aerospace Sciences Meeting*, Nashville, TN, 2021. Submitted.

[30] Seif, M. N., McDaniel, S. M., Beck, M. J., and Martin, A., "Stochastic Modeling of Elastic Behavior of Fibrous Ablators," *59th AIAA Aerospace Sciences Meeting*, Nashville, TN, 2021. Submitted.

[31] Ho, M. F., Pérez, J. G., Reggio, M., and Trépanier, J.-Y., "Permeability calculation of rarefied gasflows through 2D porous structures using the lattice Boltzmann method," *Physics and Chemistry of the Earth*, 2019. doi:10.1016/j.pce.2019.02.014.

[32] White, C., Scanlon, T. J., and Brown, R. E., "Permeability of Ablative Materials Under Rarefied Gas Conditions," *Journal of Spacecraft and Rockets*, 2016. doi:10.2514/1.A33279.